2010 IEEE International Conference on Robotics and Automation
Anchorage Convention District
May 3-8, 2010, Anchorage, Alaska, USA

Experimental Evaluation of an Autonomous Surface Vehicle for Water Quality and Greenhouse Gas Emission Monitoring

Matthew Dunbabin
Autonomous Systems Laboratory
CSIRO ICT Centre
P.O. Box 883, Kenmore, QLD 4069, Australia
matthew.dunbabin@csiro.au

Alistair Grinham
Centre for Water Studies
School of Engineering
University of Queensland
St Lucia, QLD, Australia
a.grinham@uq.edu.au

***Abstract*— This paper describes the experimental evaluation of a novel Autonomous Surface Vehicle capable of navigating complex inland water reservoirs and measuring a range of water quality properties and greenhouse gas emissions. The 16 ft long solar powered catamaran is capable of collecting water column profiles whilst in motion. It is also directly integrated with a reservoir scale floating sensor network to allow remote mission uploads, data download and adaptive sampling strategies. This paper describes the onboard vehicle navigation and control algorithms as well as obstacle avoidance strategies. Experimental results are shown demonstrating its ability to maintain track and avoid obstacles on a variety of large-scale missions and under differing weather conditions, as well as its ability to continuously collect various water quality parameters complimenting traditional manual monitoring campaigns.**

I. Introduction

This work addresses a need to improve the spatial-temporal resolution of data collected on inland water storages and lakes with the development of a unique Autonomous Surface Vehicle (ASV) (see Figure 1). The system is designed to navigate unsupervised and take precise measurements of water quality throughout the water column and greenhouse gas emissions whilst in motion.

A review of ASV technology by Caccia [1] describes how ASV prototype systems have been developed for both marine and aquatic science and military applications. The primary research areas identified in the literature has focused on vehicle design and construction [2]–[5], navigation and control [6]–[8] and path-planning and obstacle avoidance [3]. The use of multiple ASVs has been proposed to provide communication support for Autonomous Underwater Vehicles [2], [9] and formation control for marine security applications [10].

Despite the increased popularity of ASVs globally, there are limited examples of systems designed for long-duration, large-scale unsupervised environmental monitoring. A notable example is by Higinbotham et al [11] who developed and demonstrated solar powered ASVs for ocean and atmospheric observation, however, they currently have no active obstacle avoidance capability. Other examples include a wind and solar powered yacht [12] and an electric catamaran [13], both currently in the commissioning phase.

Mobile adaptive sampling is an emerging research area where the ASV can alter its trajectory to improve the measurement resolution in space and time. Zhang [14] describe their preliminary work in this area, however, their search space is relatively small and the vehicle movement is faster than the process they are trying to measure. A key motivation for the ASV presented in this paper is to develop adaptive sampling regimes for significantly larger regions where the processes are faster than the vehicles speed. Therefore, robust control and obstacle avoidance strategies are required for integration with higher level path planners.

In order to improve science delivery and operational functionality of these robots, the CSIRO Autonomous Systems Laboratory has been developing integrated marine robot and sensor network systems. These systems allow different vehicles to interact at a level to achieve complex tasks such as detect and sample events, inspection, calibration of fixed sensor nodes, and automatic retrieval of Autonomous Underwater Vehicles [15]. The work presented here builds on these systems and describes the control and operational performance of an ASV designed for long-duration missions on dynamically changing inland water storages that cover many hundreds of square kilometres.

Fig. 1. The solar-powered Lake Wivenhoe ASV.

The remainder of this paper is structured as follows; Section II provides an overview of the ASV design and system architecture. Section III describes the navigation and control strategy employed on the ASV including obstacle avoidance. Experimental results and performance analysis of the ASV during large-scale sampling missions are shown in

Section IV, with Section V concluding the paper.

II. The Lake Wivenhoe ASV

The pilot deployment sites for the ASV was on Lake Wivenhoe and Little Nerang Dam. Lake Wivenhoe is located west of Brisbane, Queensland (27.3941^{o}S 152.608^{o}E) and has surface area of 109 km^2 with a capacity of 1.16x10^6 ML of drinking water. Little Nerang Dam is located south of Brisbane (28.1479^{o}S 153.283^{o}E) and has a surface area of 0.5 km^2 and capacity of 9 280 ML.

The ASV's role is to autonomously navigate and continuously collect water quality information and relay this back to shore in real-time. A number of design and operational considerations were required in the ASV design:

- Carry a range of specialised (and often large) scientific instruments for water quality and greenhouse gas emission measurement.
- Operate continuously for 24 h from electric sources at low survey speed.
- Profile the water column whilst in motion.
- Sample at speeds from 0.5 - 3.0 ms^{-1}.
- Operate in winds up to 15 knots.
- Maintain track at speeds as low as 0.5 ms^{-1}.
- Detect a range of obstacles in the water including trees, floating nodes and buoys, boats, and canoes.
- Track and map the shoreline.
- Detect and avoid non-traversable shallow water.
- Operate without line-of-sight communications.
- Maintain minimal standoff distance (station keep) for calibration of floating sensor nodes.
- Automatically dock into a cage for safe keeping.
- Be operated manually, remotely and autonomously by non-skilled personnel.

A. System Architecture

To meet the above specifications a compromise between vehicle size, controllability and power was required. In particular, the range of sensors (navigation and scientific) and general operating conditions (waves and wind) meant that a larger stable catamaran-like vehicle would be the appropriate choice of platforms. Therefore, a low-drag 16 ft catamaran was retrofitted with a custom instrument housing containing solar panels, electric motors, navigation sensors and a profiling arm to allow measurement down to 5.5 m whilst the vehicle is moving. A further design enhancement can allow the sensor payload to be lowered to 20 m when stationary.

Figure 2 shows an overview drawing of the ASV. The vehicle has two 30 lb thrust electric motors to allow heading/tracking control at low speeds and during station keeping. It is fitted with a suite of navigation sensors which includes a GPS, compass, depth sensor, laser scanner and camera all of which interface with an onboard 1.4 GHz Pentium M processor. Communications on and off-board the ASV are typically via a wireless sensor network interface using the Fleck^{TM} sensor network board [16] as used in the floating sensor network (see Section II-B).

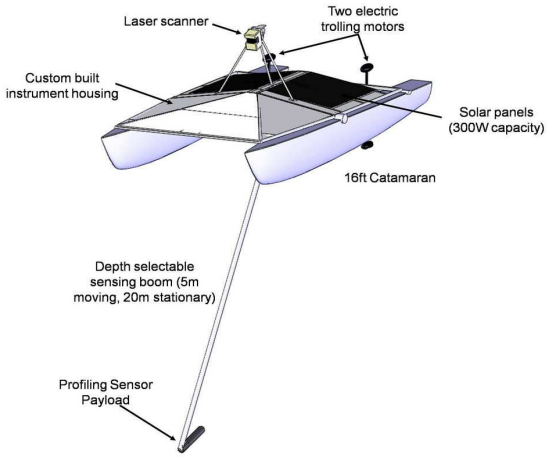

Fig. 2. Overview drawing of the 16 ft long electric profiling water quality ASV.

A typical sensor payload for the ASV consists of an Optical Methane Detector (OMD, Heath Consultants, Texas), YSI Sonde (measuring temperature, conductivity, chlorophyll, turbidity, dissolved oxygen), wind sensor and a profiling sonar. Details of the ASV systems and further functionality are described in [17].

B. Sensor network integration

The ASV is designed to interface directly with static and mobile sensor networks for operational and communication support. A 50 node floating sensor network based on the Fleck^{TM} wireless sensor network devices has been deployed across Lake Wivenhoe measuring temperature down the water column [18]. The continuous monitoring of these nodes enables early detection of events, such as algal blooms, and validation of modelling and prediction against the incoming data.

The ASV can use the sensor network for two-way communications to network nodes and operators beyond direct line-of-sight. Remote Procedural Calls (RPCs) are used to action the ASV to perform particular tasks. Typical tasks relate to internode sampling, event analysis, as well as in-situ calibration of the floating sensor nodes. Figure 3 shows the ASV with one of the Lake Wivenhoe sensor nodes in the background.

III. Navigation & Control

At the highest level, missions are specified as a series of waypoints and segment velocities with functionality tags (such as profile, station keep, dock). The vehicle attempts to maintain a straight path between successive waypoints, however, this can be modified with the detection of obstacles and shallow non-traversable water.

A particular challenge with this ASV is controllability at low speed as the control effectiveness of rudders is proportional to the square of velocity. At relatively low survey speeds (less than 1.0 ms^{-1} to allow water quality sensor equilibration), this requires the vehicle use a combination of control inputs such as differential thrust from the two electric

Fig. 3. The ASV is integrated with an array of 50 floating sensor network nodes (orange buoy behind the ASV) for communication and event detection. The ASV is capable of detecting a node and maintaining a minimal stand off distance to allow in situ calibration of the nodes sensors.

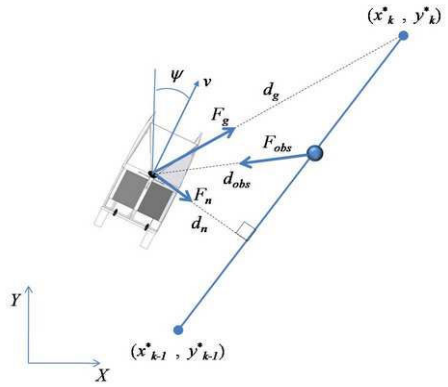

Fig. 4. Virtual forces acting on the ASV during normal operation when moving from path coordinates (x^*_{k-1}, y^*_{k-1}) to (x^*_k, y^*_k) at speed v^*_k.

motors as well as rudder deflection to maintain track. As the vehicle is propelled by only two 30 lb thrust electric motors, its control authority is relatively low with respect to the mass of the ASV. This has had a strong influence on the controller design and tracking performance presented in later sections.

A. Pose Estimation

The vehicle's pose consists of a 2D position (x, y) which is aligned with a grid coordinate system (Eastings and Northings), its velocity (v) and heading angle (ψ) referenced to true North, as well as the track bearing (ϕ). Additionally, the depth under keel (z_{uk}) and tiller angle (δ) are added to the pose vector for use in the controller.

Roll and pitch are ignored on the current ASV as although the lake can experience wave heights of approximately 0.5 m, the catamaran design remains relatively stable.

The pose elements x, y, v and ϕ are obtained from the on-board GPS (non-differential) at an update rate of 4 Hz and fused with a digital compass (ψ) at a rate of approximately 2 Hz using a Kalman filter with a constant velocity vehicle model. A profiling sonar is used to measure z_{uk} at 1 Hz.

B. Virtual Force Control

Virtual forces were chosen for the ASV navigation as they offer a relatively simple method of directing the vehicle towards a goal point with the ability to include static and dynamic obstacles. A number of novel features were developed to allow the vehicle to avoid running aground (track towards the deep water channel), as well as to simply, but indirectly, specify the desired tracking accuracy during waypoint and docking control.

The total control force vector acting on the ASV (F_c) consists of an attraction force (F_g) pulling the vehicle towards the goal location, an alignment force (F_n) to bring the vehicle on a straight line track between the start and goal locations, and an repelling force (F_{obs}) centred on each known or sensed obstacle. Figure 4 illustrates the typical virtual forces acting on the ASV.

The attracting goal force is determined by:

$$F_g = \left(\frac{2u_{max}}{r_g}\right) d_g \tag{1}$$

where u_{max} is the maximum individual motor control input (assumed constant for each motor), r_g is a radius around the goal location whereby the vehicle begins to slow down, and d_g is the Euclidean distance between the current ASV position and the goal location (x^*_k, y^*_k). This attraction force acts directly from the ASV to the goal location at angle ψ_g.

The virtual force required to align the ASV onto the desired straight line path is determined by calculating the perpendicular (shortest) distance to the current path segment, d_n, shown in Figure 4. This alignment force, F_n is assumed a quadratic well-like surface such that:

$$F_n = F_a \ (w_n \ d_n)^2 \tag{2}$$

where w_n is a scale factor (termed here as the alignment gain) to modify the tracking performance of the ASV and F_a is a constant of proportionality. Increasing w_n improves tracking performance, however, it can also increase the energy demands to remain on track during strong wind. In practice, w_n is varied based on the functionality tag in the mission segment description. This alignment force acts at an angle ψ_n perpendicular towards the desired track.

The total control force vector, F_c, consists of the following Cartesian components:

$$F_{c_x} = F_g \sin(\psi_g) + F_n \sin(\psi_n) + F_{obs_x} \tag{3}$$
$$F_{c_y} = F_g \cos(\psi_g) + F_n \cos(\psi_n) + F_{obs_y} \tag{4}$$

where the obstacle force components (F_{obs_i}) are described in the following section.

C. Obstacles

The ASV is capable of detecting a range of static or slow moving (less than 0.5 ms^{-1}) obstacles including the shoreline, trees, floating sensors nodes and pontoons up to a nominal maximum speed of 3 ms^{-1}. The onboard laser, camera and sonar systems are used to determine the

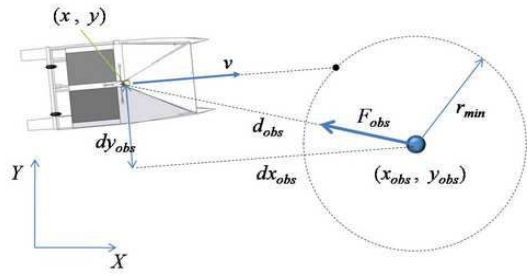

Fig. 5. Schematic showing the virtual forces which act upon the ASV when approaching an obstacle at speed v.

presence and location of these obstacles. The details of obstacle detection are not presented in this paper, however, it is assumed here that the coordinates of each obstacle are known, either a-priori or sensed in real-time.

Obstacles are represented as repelling forces with magnitude proportional to the inverse square of the distance to the obstacle and a compensation term for the relative movement between the ASV and obstacle. Figure 5 illustrates the forces and notation associated with the interaction of the ASV and an obstacle.

Given the global coordinates of an obstacle $(x_{obs_i}\ ,\ y_{obs_i})$, the static repelling force from obstacle i is given by:

$$F_{obs_i} = \frac{F_o}{d^2_{obs_i}} \tag{5}$$

where d_{obs_i} is the Euclidean distance between the ith obstacle coordinates and the vehicle, and F_o is a constant of proportionality. The bearing angle between the ith obstacle and the vehicle is denoted by ψ_{obs_i}.

If the vehicle anticipates it will encroach a prespecified exclusion zone around an obstacle, r_{min}, it modifies its path (generally towards the deep water channel) until clear of the obstacle and then resumes tracking the desired path. Modification of the path for the ASV travelling at speed (v) with a relative velocity to the obstacle (v_x, v_y) is obtained by:

$$\theta_{v_i} = \cos^{-1}\left(\frac{v_x(x_{obs_i} - x) + v_y(y_{obs_i} - y)}{d_{obs_i}\ v}\right) \tag{6}$$

$$dx_{obs_i} = d_{obs_i}\cos(\theta_{v_i}) \tag{7}$$

$$dy_{obs_i} = d_{obs_i}\sin(\theta_{v_i}) \tag{8}$$

To determine if a collision will occur, the following conditions are required $((r_{min} - |dy_{obs_i}|) > 0)$ and $(\cos\theta_{v_i} > 0)$, then the time to impact (t_c) is:

$$t_c = \frac{dx_{obs_i}}{v} \tag{9}$$

and the velocity compensated force component is given by:

$$F_{v_i} = \left(\frac{F_o}{t_c^2}\right)\ (r_{min} - |dy_{obs_i}|) \tag{10}$$

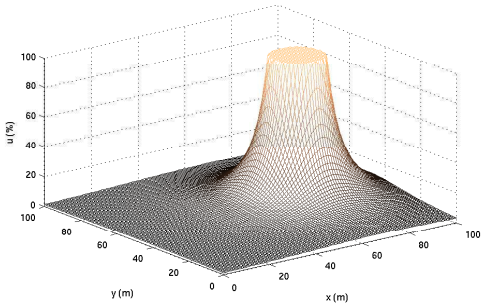

(a) Repelling force for a static obstacle and ASV.

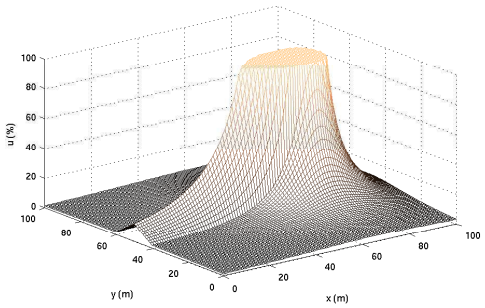

(b) Repelling force with the ASV moving at $v_x = 1$ ms^{-1}.

Fig. 6. Repelling control force magnitude for a static obstacle and with a velocity compensation. Obstacle location at $(70, 50)$ and r_{min} = 10 m.

Therefore, the total velocity compensated obstacle force components acting on the ASV are:

$$F_{obs_x} = \sum_{i=1}^{n}(F_{obs_i} + F_{v_i})\sin(\psi_{obs_i}) \tag{11}$$

$$F_{obs_y} = \sum_{i=1}^{n}(F_{obs_i} + F_{v_i})\cos(\psi_{obs_i}) \tag{12}$$

Figure 6 shows the effect of including the approach velocity of the ASV on a static obstacle.

D. Vehicle Control

The controlled variables for the ASV are the desired velocity for the kth mission segment (v_k^*), the vehicle heading (ψ_t^*), and the tiller angle (δ^*). A modification to the desired segment velocity is performed to reduce the vehicle's speed close to the goal location such that:

$$v_{scale} = \begin{cases} d_g/r_g & if\ (d_g < r_g) \\ 1 & otherwise \end{cases} \tag{13}$$

where r_g is a radius around the goal location whereby the vehicle begins to slow down. Therefore, the demanded velocity is then determined by:

$$v^* = v_k^*\ v_{scale} - (1 - v_{scale})\ v \tag{14}$$

The desired vehicle bearing is obtained from Section III-B such that:

$$\psi_t^* = \tan^{-1}\left(\frac{F_{c_x}}{F_{c_y}}\right) \tag{15}$$

Proportional controllers are used to calculate heading control inputs for the tiller (δ^*) and motors (u_ψ^*) such that:

$$\delta^* = K_{p_\delta}(\psi_t^* - \psi) \tag{16}$$
$$u_\psi^* = K_{p_\psi}(\psi_t^* - \psi) \tag{17}$$

where K_{p_ψ} and K_{p_δ} are proportionality gains.

The proposed controller has preference for heading control, therefore, the amount of control authority available for velocity control is given by:

$$u_{v_{max}} = 2u_{max} - \left|u_\psi^*\right| \tag{18}$$

where $(0 \leq u_{v_{max}} \leq 2u_{max})$.

Therefore, the velocity command is determined by:

$$u_v^* = K_{f_v} v^* + K_{i_v} \int (v^* - v)\, dt \tag{19}$$

where $(-u_{v_{max}} \leq u_v^* \leq u_{v_{max}})$.

Finally, the drive commands for the two motors and tiller actuator $(u_L^*, u_R^*, u_\delta^*)$ to maintain the controlled variables are:

$$u_L^* = \left(u_v^* + u_\psi^*\right)/2 \tag{20}$$
$$u_R^* = \left(u_v^* - u_\psi^*\right)/2 \tag{21}$$
$$u_\delta^* = K_{p_{\delta_u}}(\delta^* - \delta) \tag{22}$$

Each of the motor commands are then clipped to their safe operational range $(u_{min_i} \leq u_i^* \leq u_{max_i})$.

IV. Experimental Results

The ASV has undergone extensive field trials to evaluate the tracking and obstacle avoidance performance in a variety of weather conditions and operational scenarios. The control gains were selected through experimentation to achieve the desired tracking performance with significant cross winds whilst considering the ASV's limited control authority as well as minimising energy expenditure to maximise endurance.

Figure 7 shows a case study whereby the ASV conducted a circuit with a "standard" and a "higher" precision alignment gain at 1.0 ms^{-1}. The average wind speed was 15 knots with gusts up to 25 knots during the experiment. The mean tracking error was 6.2 m and 2.9 m for the standard and high gains respectively with the higher gain requiring 18% more power compared to the standard gain.

The tracking performance of the ASV with different alignment gains and wind disturbances is illustrated in Figure 8. In this figure, the ASV's speed was commanded to 1.0 ms^{-1} (survey). For the relatively low-power "standard" alignment gain the tracking error is within 10 m under wind conditions of 10-20 knots (Figure 8(a)). The tracking error is reduced to 2 m with a higher "precision" track alignment gain (Figure 8(b)). Figure 8(c) shows the tracking error with

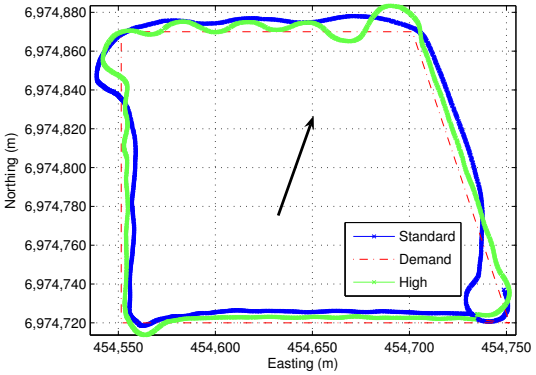

Fig. 7. Measured trajectory of the ASV with different tracking alignment gains (without profiling boom). The mean wind speed was 15 knots with gusts up to 25 knots during the experiment in the direction shown by the arrow.

standard gain for the mission shown in Figure 10 whilst profiling the water column down to 4.5 m with a period of 5 minutes illustrating general consistency with Figure 8(a).

Figure 9 shows two measured obstacle avoidance manoeuvre trajectories with the ASV travelling at 0.9 ms^{-1} using the method described in Section III. The obstacle, a floating sensor node, was detected using the laser scanner and the required safety exclusion zone was set at a radius of 15 and 10 m for Figures 9(a) and (b) respectively. Note that the minimum turning radius of the ASV whilst moving is approximately 20 m. As shown in Figure 9, the ASV was capable of localising the obstacle and modifying its trajectory to maintain the safe distance from the obstacle and then realigning with the desired path.

The long term performance of the entire system has been evaluated by conducting repeat sampling missions using the profiling sensor arm and surface OMD. Figure 10(a) shows the actual trajectory of a 3 km mission conducted on Lake Wivenhoe during early morning July 2009. The temperature and dissolved oxygen traces (Figure 10(c & d)) 1.5 and 4 m below the surface, show a general increase in both parameters as the ASV moves towards the open channel (as seen by the depth trace (Figure 10(b)).

The ability to generate spatial-temporal maps of greenhouse gas emissions using the ASV were evaluated on Little Nerang Dam. Figure 11(a) shows a measured surface methane concentration distribution using the OMD attached to the ASV. Figures 11(b) and (c) show the measured methane concentration along a repeat ASV transect (shown in Figure 11(a)) illustrating a spatial-temporal variation of methane flux.

V. Conclusions

A unique Autonomous Surface Vehicle (ASV) capable of navigating complex inland water storages has been presented. The custom built solar powered catamaran is capable of collecting various water quality measurements by moving a sensor payload up and down the water column whilst in

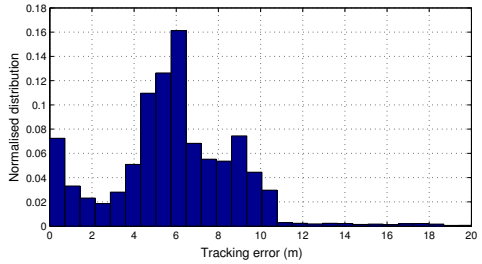

(a) Standard precision tracking gain (transect distance 27 km)

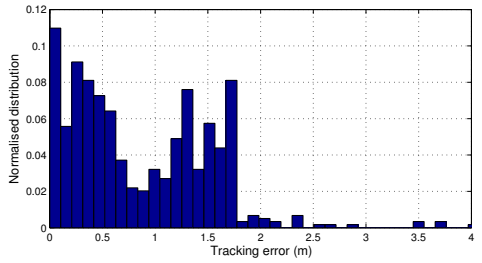

(b) High precision tracking gain (total transect distance 2 km)

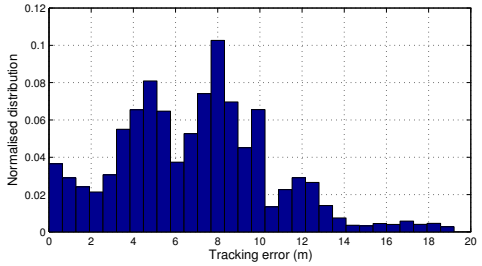

(c) Tracking error when profiling the water column with standard gain for the mission shown in Figure 10

Fig. 8. Normalised tracking error distribution for combined missions and variable wind speeds up to 20 knots. (a) and (b) are without profiling (sensing) arm deployed and (c) is with profiling arm deployed.

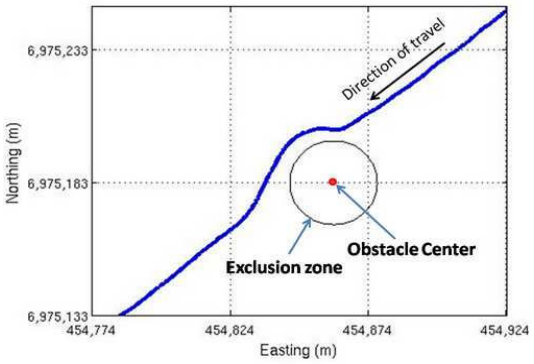

(a) ASV path offset from obstacle ($r_{min} = 15$ m).

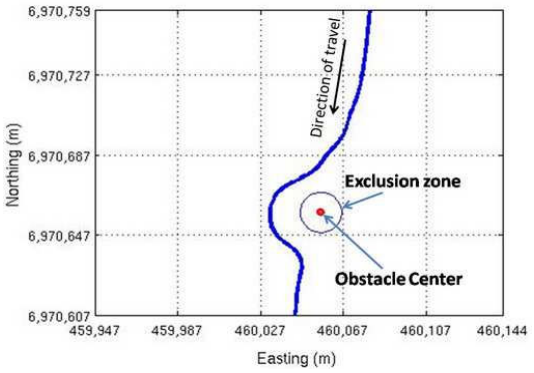

(b) ASV path in direct line of obstacle ($r_{min} = 10$ m). The effect of velocity compensation is evident with the ASV deviating as it approaches the obstacle.

Fig. 9. Measured ASV trajectories after detection of an obstacle whilst travelling at 0.9 ms^{-1}. The maximum obstacle detection range was 30 m.

motion, as well as measuring the spatial-temporal release of various greenhouse gas emissions. The integration of onboard sensors including a GPS, laser scanner, sonar and camera allow the ASV to operate successfully in previously unmapped shallow water environments, as well as avoid static and mobile obstacles on the surface. The vehicle's control and obstacle avoidance strategies are based on virtual forces and have proven robust and consistent in field experiments. Extensive field trials have demonstrated the vehicle's ability to maintain repeatable transects over large distances and variable weather conditions, as well as detect and avoid a range of obstacles. The data collected by the ASV is complementing existing manual monitoring campaigns with improved spatial and temporal monitoring of the water storage with hundreds of kilometres of survey and missions up to 24 hours duration already completed.

Acknowledgements

This work was jointly funded by Seqwater and the CSIRO Sensor & Sensor Network Transformational Capability Platform. The authors would like to thank Brett Wood, Ben Mackey, Les Overs and John Whitham from the CSIRO ICT Centre Autonomous Systems Laboratory, and Dr James Udy and Deb Gale from Seqwater for their contributions during construction and field evaluation of the system.

REFERENCES

[1] M. Caccia, "Autonomous surface craft: prototypes and basic research issues," in *Proc. 14th Mediterranean Conference on Control and Automation*, June 2006, pp. 1–6.

[2] J. Curcio, J. Leonard, and A. Patrikalakis, "SCOUT - a low cost autonomous surface platform for research in cooperative autonomy," in *Proc. MTS/IEEE OCEANS 2005*, September 2005, pp. 725–729.

[3] J. Larson, M. Bruch, and J. Ebken, "Autonomous navigation and obstacle avoidance for unmanned surface vehicles," in *Proc. SPIE Unmanned Systems Technology VIII*, April 2006.

[4] A. Leonessa, J. Mandello, Y. Morel, and M. Vidal, "Design of a small, multi-purpose, autonomous surface vessel," in *Proc. OCEANS 2003*, 2003, pp. 544–550.

[5] C. Reed, B. Bishop, and J. Waters, "Hardware selection and modelling for a small autonomous surface vessel," in *Proc.38th Southeastern Syposium on System Theory*, March 2006, pp. 196–200.

[6] T. Vaneck, "Fuzzy guidance controller for an autonomous boat," *Control Systems Magazine*, vol. 17, pp. 43–51, 1997.

[7] J. Alves, P. Oliveira, R. Oliveira, A. Pascoal, M. Rufino, L. Sebastiao, and C. Silvestre, "Vehicle and mission control of the DELFIM autonomous surface craft," in *Proc. 14th Mediterranean Conference on Control and Automation*, June 2006, pp. 1–6.

[8] M. Reyhanoglu and A. Bommer, "Tracking control of an underactuated autonomous surface vessel using switched feedback," in *Proc. IECON 2006*, November 2006, pp. 3833–3838.

[9] J. Curcio, J. Leonard, J. Vaganay, and A. Patrikalakis, "Experiments in moving baseline navigation using autonomous surface craft," in *Proc. MTS/IEEE OCEANS 2005*, September 2005, pp. 730–735.

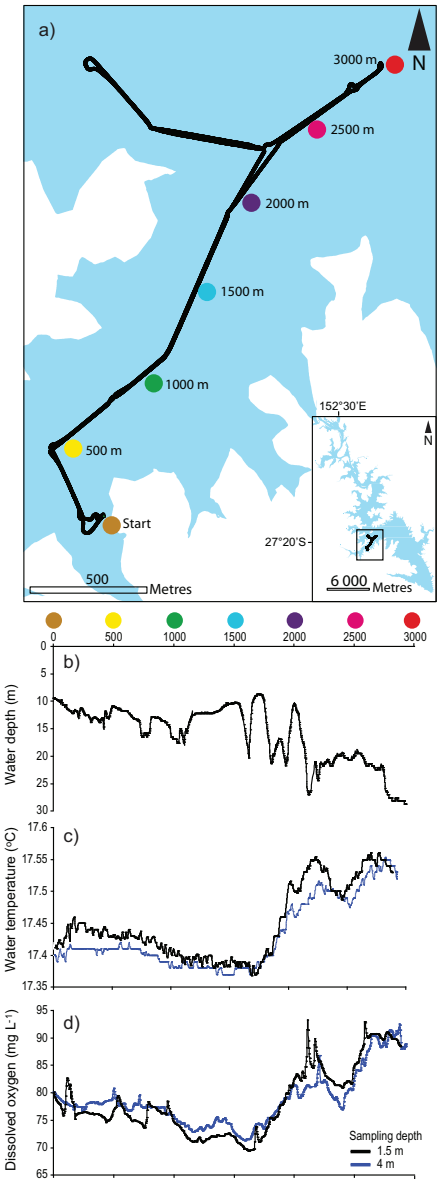

Fig. 10. Measured trajectory of the ASV and water temperature using the profiling sensor arm during a dawn sampling mission. These results were taken in conjunction with an annual manual sampling campaign and demonstrated consistency of measurement and improved spatial-temporal distribution and repeatability. The straight line trajectory can be seen to be locally modified as a result of obstacle avoidance with floating sensor nodes (for example between 2500 and 3000 m).

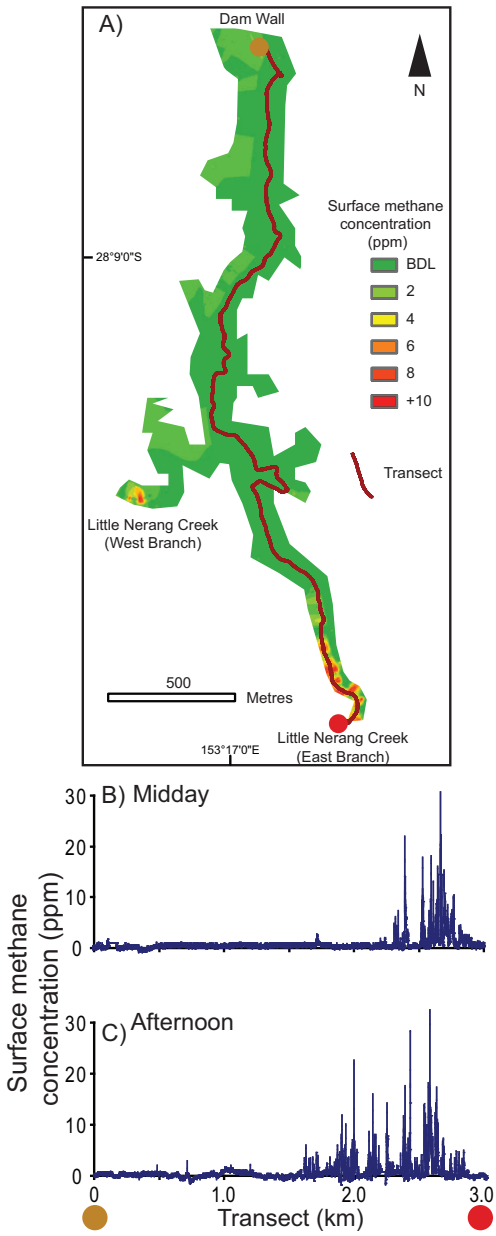

Fig. 11. A measured atmospheric methane distribution graph and variation along the same track with time of day using the Optical Methane Detector on the ASV for Little Nerrang Dam in Queensland Australia.

[10] B. Bishop, "Design and control of platoons of cooperating autonomous surface vessels," in *Proc. 7th Annual Maritime Transportation System Research and Technology Coordination Conference*, November 2004.

[11] J. Higinbotham, J. Moisan, C. Schirtzinger, M. Linkswiler, J. Yungel, and P. Orton, "Update on the development and testing of a new long duration solar powered autonomous surface vehicle," in *Proc. IEEE OCEANS 2008*, September 2008, pp. 1–10.

[12] P. Rynne and K. von Ellenrider, "A wind and solar-powered autonomous surface vehicle for sea surface measurements," in *Proc. IEEE OCEANS 2008*, September 2008, pp. 1–6.

[13] J. Wang, W. Gu, and J. Zhu, "Design of an autonomous surface vehicle used for marine environmental monitoring," in *Proc. International Conference on Advanced Computer Control (ICACC09)*, January 2008, pp. 405–409.

[14] B. Zhang and G. Sukhatme, "Adaptive sampling for estimating a scalar field using robotic boat and a sensor network," in *Proc. International Conference on Robotics and Automation*, April 2007, pp. 3673–3680.

[15] M. Dunbabin, B. Lang, and B. Wood, "Vision-based docking using and autonomous surface vehicle," in *Proc. International Conference on Robotics and Automation*, May 2008, pp. 26–32.

[16] P. Corke, P. Valencia, P. Sikka, T. Wark, and L. Overs, "Long-duration solar-powered wireless sensor networks," in *Proc. Emnets*, June 2007.

[17] M. Dunbabin, A. Grinham, and J. Udy, "An autonomous surface vehicle for water quality monitoring," in *Proc. Australasian Conference on Robotics and Automation*, December 2009.

[18] M. Dunbabin, J. Udy, A. Grinham, and M. Bruenig, "Continuous monitoring of reservoir water quality: The Wivenhoe project," *Water*, vol. 36, pp. 74–77, September 2009.